Tellus (2000), 52B, 1216–1231
Printed in UK. All rights reserved

TELLUS
ISSN 0280–6509

A physically-based algorithm for estimating the relationship between aerosol mass and cloud droplet number

By PAUL GLANTZ* and KEVIN J. NOONE, *Department of Meteorology, Stockholm University, 106 91 Stockholm, Sweden*

(Manuscript received 31 March 1999; in final form 27 March 2000)

ABSTRACT

In this study, we present a relationship between total accumulation mode aerosol mass concentrations and cloud droplet number concentrations (N_d). The fundamental aim with the present method is to arrive at a physically-based conversion algorithm in which each step in the conversion is based on real physical processes that occur and can be observed in the atmosphere, and in which all of the fields involved can be observed or modeled. In the last conversion (the critical part in the algorithm), we use measurements of the size distributions of cloud droplet residual particles for different pollution conditions. This conversion assumes that the size of the residual particles can be described with a lognormal distribution function and uses the Hatch–Choate relationship to convert between residual volume and number. The relatively sparse data set with which we have developed the present algorithm results in a course classification of the aerosol mass field. Consequently, uncertainties need to be recognized when using the algorithm in its present form in model calculations. The algorithm has been used on data from 15 days and the agreement between calculated and observed N_d values is, with one exception, within a factor of 2 and for many of these cases also much better than a factor of 2. In addition to the results of the algorithm itself, we also present a least-squares fit to the predicted N_d values. To improve the algorithm in the longer-term requires more data of scavenging fractions, particle chemical composition and density, and residual particle size distributions as a function of aerosol mass loading and cloud type.

1. Introduction

Aerosol particles in the atmosphere have a potential impact on the Earth's radiation balance and also on global climate. These effects occur both directly and indirectly. Direct forcing, due to an increase of man-made aerosol particles in the cloud-free atmosphere, results in increased scattering of radiation back to space. The total direct forcing due to sulfate, fossil fuel soot and organic aerosols from biomass burning is estimated to be $-0.5\ \mathrm{W\,m^{-2}}$, with a range of -0.25 to $-1.0\ \mathrm{W\,m^{-2}}$ (IPCC, 1995). Similarity the indirect effect, an increase of anthropogenic aerosols leading to increased cloud droplet concentrations, is assumed to have a positive influence on cloud albedo (Twomey, 1977; Twomey et al., 1984). It has also been suggested that anthropogenic aerosols can alter the extent of cloudiness (Albrecht, 1989). The estimation of the radiative forcing due to changes in cloud properties is between 0 and $-1.5\ \mathrm{W\,m^{-2}}$ (IPCC, 1995). The uncertainties in the estimation of the indirect forcing are much larger than the uncertainties in the estimation of the direct forcing (IPCC, 1995).

The geochemical cycles for species that compose

* Corresponding author.
e-mail: paul.glantz@misu.su.se

atmospheric aerosols are of necessity formulated in terms of aerosol mass in climate models. A key problem in the estimation of the indirect effect with present global scale models is to find a relationship/link between aerosol mass and cloud droplet number concentrations (N_d), in which the important physical/chemical processes that link these two quantities are adequately described. Slingo (1990) has used a general circulation model (GCM) to study the sensitivity of the climate to changes in the properties of low-altitude clouds. Their results give an indication of the accuracy required by using an algorithm to estimate/calculate N_d. If the liquid water path were constant, he found that a decrease of 15 to 20% in the mean particle radius (which corresponds to an increase in the number of cloud droplets of between 60 to 102%) is needed to offset the top of the atmosphere radiative impact of a doubling of carbon dioxide (about 2.5 W m^{-2}). This study indicates that the accuracy in the results of calculated N_d must be much better than a factor of 2 to be useful in climate modelling.

Several authors have estimated relationship between non-sea salt sulfate mass and cloud droplet concentrations. Jones et al. (1994) have estimated a relationship between N_d and total accumulation mode aerosol number concentrations (N_a), based on observations from Martin et al. (1994). The estimated relationship is nearly linear for maritime conditions but becomes nonlinear for more polluted conditions. By assuming that all aerosol particles are ammonium sulfate with a fixed spectral shape Jones and Slingo (1996) estimated a relationship between sulfate mass and N_a. Based on these assumptions Jones and Slingo have then estimated a relationship between cloud droplet and sulfate mass concentrations. These results are compared with two other empirical parameterisations, first presented in Jones and Slingo (1996), by Hegg (1994) and Boucher and Lohmann (1995). The two latter works do not assume that all aerosol particles are ammonium sulfate but instead assume only a link between N_d and sulfate mass concentrations.

There are problems in both approaches described above to estimate N_d. For present-day conditions sulfate is the most approachable component to model but not necessarily the only appropriate one. The method used by Jones et al. is limited because only sulfate aerosols are represented in the conversion from $SO_4^=$-mass to N_a, and various studies have shown that sulfate is not the only aerosol component of importance in droplet nucleation (Hegg et al., 1993, 1995; Novakov and Penner, 1993; Noone et al., 2000; O'Dowd and Smith, 1993; Rivera-Carpio et al., 1996; Russel et al., 2000). The approach worked out by Hegg, and Boucher and Lohmann would seem to circumvent these problems by assuming a link exclusively between N_d and sulfate mass. However, a problem with this latter approach is that this link could be weak (Hegg et al., 1993, 1995; Novakov and Penner, 1993; Rivera-Carpio et al., 1996).

In this paper, a relationship between cloud droplet number and total accumulation mode mass concentrations will be presented. In contrast to the approaches described above the present method is based on a physically-based conversion algorithm which includes (at least and as a first step) a description of some of the real physical processes that occur in the atmosphere. A description of the method used to estimate this relationship will be presented in Section 2. Brief descriptions of the instrumentation used in this study and the operation areas from which observations have been analysed are found in Section 3. In Section 4 estimationsof the four fields which constitute the present algorithm will be presented. In Section 5 the results of calculated N_d will be compared with simultaneous independent measurements of N_d using measurements from the Meteorological Research Office's (MRF) C-130 research aircraft, University of Washington's (UW) C-131 research aircraft and data from Noone et al. (1992). The present results are also compared with studies by Boucher and Lohmann, Hegg, and Jones and Slingo in Section 5. Finally, summary and conclusions are presented in Section 6.

2. Methodology

Fig. 1 is an illustration of the logic we will use in this study to estimate a relationship between total accumulation mode aerosol mass concentrations (M_{amp}) and N_d. We will also consider the uncertainties involved in each of these steps. The fundamental aim with this method is to arrive at a physically-based conversion algorithm in which

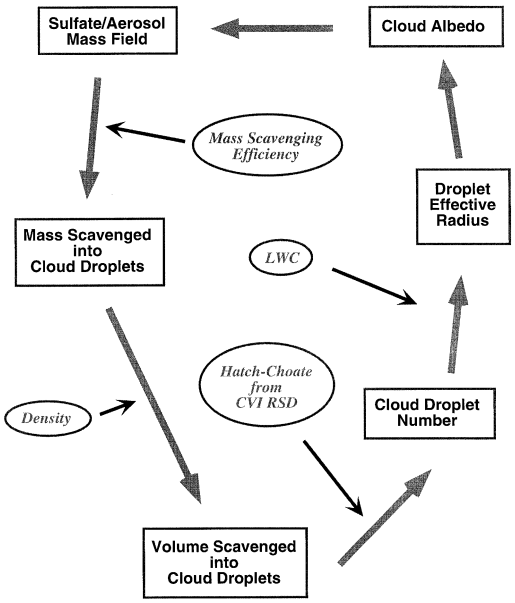

Fig. 1. An illustration of the logic used in the algorithm to estimate a relationship between aerosol mass and cloud droplet number. The first four fields and three conversions are the subject of this paper. The remaining fields and conversions will be the subject of subsequent investigations.

each step in the conversion is based on real physical processes that occur and can be observed in the atmosphere, and in which all of the fields involved can be observed or modeled. The rectangular boxes in Fig. 1 represent fields and the ovals represent conversions between the fields.

The first conversion in the algorithm involves calculating the amount of available aerosol mass that is actually taken up in the cloud droplets. This process is denoted by the "mass scavenging efficiency" oval in Fig. 1. Mass scavenging efficiencies for accumulation-mode aerosols in clean conditions are close to unity, while in more polluted locations mass scavenging efficiencies can be quite low (a detailed description of the mass scavenging efficiencies and the corresponding uncertainties used in this study is presented in Subsection 4.2). Applying this conversion to the aerosol mass field allows us to calculate the second field in the method — the aerosol mass scavenged into cloud droplets.

We begin with an aerosol mass field — either total accumulation-mode mass or accumulation-mode sulfate mass. We concentrate on the accumulation-mode, since typical supersaturations in most clouds are not sufficiently large to activate particles in the smaller modes, and since coarse-mode particles rarely contribute more than ca. 10% to the total aerosol particle number concentration.

Most model studies of the indirect radiative effect of aerosols to date have used sulfate fields as inputs, since our understanding of this particular component is better than for most of the other constituents that make up atmospheric aerosols. In reality, particles other than sulfate can also cause cloud droplet formation (Hegg et al., 1993, 1995; Novakov and Penner, 1993; Noone et al., 2000; Russell et al., 2000). A correct description of the relationship between aerosol mass and cloud albedo will therefore require use of the total M_{amp}, not just the sulfate component. We should note, however, that the method we derive could still be used to estimate what changes in cloud albedo may have arisen due to anthropogenically-produced sulfate particles, but that this albedo change may not reflect the total change in cloud albedo due to anthropogenic activity, since human activity also produces other kinds of particles.

Once we know how much of the available aerosol mass is found in the cloud droplets, we can use a value of density for the particles to calculate the third field — the volume of aerosol contained in the cloud droplets. The uncertainties involved in estimating density for a multicomponent, potentially externally-mixed aerosol are discussed in Subsection 4.3. From the volume of aerosol scavenged into cloud droplets we can use measurements of the size distributions of cloud droplet residual particles (RSDs) for different pollution conditions to convert between scavenged aerosol volume to residual particle (thus cloud droplet) number concentrations. This conversion assumes that the size of the residual particles can be described with a lognormal distribution function and uses the Hatch–Choate relationships for lognormal distributions to convert between residual volume and number. Using this conversion, we can calculate the cloud droplet number field.

These first 4 fields and three conversions will be the subject of this paper. There are 2 additional fields and conversions shown in Fig. 1 — estimating the field of cloud droplet effective radius from cloud droplet number and liquid water content,

and finally to calculate the cloud albedo from the effective radius. These fields and conversions will be the subject of subsequent investigations. Here, we present the algorithm to convert between aerosol mass and cloud droplet number.

3. Experimental

A counterflow virtual impactor (CVI) has been used to obtain information about the relationship between scavenged aerosol mass and cloud droplet number. Using the CVI, cloud droplets are separated from the ambient air into a dry particle-free carrier air stream. In the CVI system the cloud droplets are heated and evaporated. The water and any volatile species dissolved in the droplets are driven into the gas phase, while the non-volatile species are measured as cloud droplet residual particles. Each droplet after evaporation is assumed to release one particle. Outside cloud the CVI was deployed as a "normal" aerosol inlet which means that air was aspirated directly into the system. The residual or out-of-cloud aerosol particles where then measured with a Particle Measuring System (PMS) Passive Cavity Aerosol Spectrometer Probe (PCASP) with a size range from 0.11 to 9 μm in diameter. Residual and out-of-cloud particles were also collected on filters for analysis by ion chromatography. A more detailed description of the CVI could be found in Ogren et al. (1985) and Noone et al. (1988).

Data from several locations are included in this study. Land-based measurements carried out pre-fog and in fog conditions in November 1989 outside San Pietro Capofiume in the Po Valley have been used. The Po Valley is the largest industrial and agricultural area in Italy and can be considered as a highly polluted continental location. Aircraft measurements have been analysed from the Monterey Area Ship Track (MAST) experiment carried out in the summer of 1994 in the maritime atmosphere outside of Monterey, California. The observations taken from MAST were performed in boundary layer stratiform clouds characterized as "clean" conditions. Data from one flight in stratocumulus clouds over the North Sea in March 1997 have also been used. Here, the maritime atmosphere was influenced by polluted air advected from Great Britain. Finally, aircraft measurements from the North Atlantic Regional Aerosol Characterisation Experiment (ACE-2), carried out in the summer of 1997 between the coasts of Portugal, North Africa and the Canary Islands are also included in this study. The observations taken from ACE-2 were performed in clean to intermediately polluted conditions.

4. Fields and conversions estimations

4.1. Accumulation-mode mass field

The geochemical cycles for species that compose atmospheric aerosols are of necessity formulated in terms of aerosol mass in present models. Global scale models today use sources and sinks formulated for aerosol mass to predict climate change. Thus, to estimate indirect forcing by aerosols it is necessary to make an assumption about a specific relationship between aerosol mass and number concentrations. An internally consistent data set that can be used to establish this kind of relationship requires at a minimum simultaneous measurements of aerosol mass and number. Table 1 shows typical values of average number and mass concentrations of the major aerosol types (Seinfeld and Pandis, 1998). The most useful data would include measurements of aerosol mass, volume and number size distributions.

While there are a considerable number of publications concerning measurements of aerosol mass concentrations for various species, relatively few contain both mass and number, and even fewer provide simultaneous observations of aerosol number, volume and mass (Quinn et al., 1995). We will concentrate on these latter data sets in developing our algorithm.

Table 1. *A summary of typical values of average number and mass concentrations of the major aerosol types (Seinfeld and Pandis, 1998)*

Type	No. (cm^{-3})	PM_1 ($\mu g\ m^{-3}$)	PM_{10} ($\mu g\ m^{-3}$)
urban (polluted)	10^5–4×10^6	30–150	100–300
marine	100–400	1–4	10
rural	2000–10,000	2.5–8	10–40
remote continental	50–10,000	0.5–2.5	2–10

Table 2. *Estimated/measured M_{amp} are subdivided with respect to the level of anthropogenic influence*

M_{amp} classification ($\mu g\ m^{-3}$)		Location[a]	Observed N_{amp} (cm^{-3})	Converted V_{amp} ($\mu m^3\ cm^{-3}$)	Estimated ρ_{amp} ($g\ cm^{-3}$)	Conv./Obs. M_{amp} ($\mu g\ m^{-3}$)	Ref.[b]
0–2	clean conditions	NP, NA	<500	0.2–1	1.7	0.3–2	PW
		CP, NP	86, 114	0.5, 0.7	1.7	0.8[c], 1.2[c]	Q
		WM	306 ± 113			2.4 ± 1.3	PVV
2–15	intermediately polluted conditions	NA	500–900	4–6	1.6	7–10	PW
		WM	670 ± 118			6.5 ± 3.9	PVV
15–50	moderately polluted conditions	NS	1178 ± 112	16	1.6	26	PW
		WM	1777 ± 572			17.5 ± 11	PVV
>50	highly polluted conditions	PV	>3000			93 and 179	H and N

Motivation for using the mean particle density corresponding to a classification in the convertions from V_{amp} to M_{amp} is given in Subsection 4.3.
[a] NP = Northeast Pacific, NA = Northeast Atlantic, CP = Cheeka Peak (background NP site), NS = North Sea, WM = Whiteface Mountain (New York), PV = Po Valley (Italy). [b] PW = Present work, Q = Quinn et al. (1995), PVV = Pueschel and Van Valin (1986), H = Hallberg et al. (1992), N = Noone et al. (1992). [c] The assumed ρ_{amp} used in these conversions might be too high (*Q*).

Table 2 shows estimated/measured M_{amp} subdivided with respect to the level of anthropogenic influence. The locations from which the data were obtained are also shown in Table 2. Observations of total accumulation-mode volume concentrations (V_{amp}) have been converted to M_{amp}. Motivation for the values of density used in these conversions is given in Subsection 4.3. For the highly polluted cases (Po Valley) measured total interstitial mass concentrations (Hallberg et al., 1992) in combination with estimated volume/mass scavenging fractions (Noone et al., 1992) are used to estimate the M_{amp}. Due to the limited number of available measurements, the data used in the present approach are subdivided into only 4 classifications. The borders between the classifications are arbitrary; the consequences of these limitations will be discussed in Subsection 5.4.

4.2. Mass scavenging efficiency

After classifying an initial aerosol mass field, the first conversion in the algorithm entails calculating the fraction of the aerosol mass that is taken up in the cloud droplets — the scavenged fraction.

Table 3 shows some published data of accumulation-mode particle mass and number scavenging fractions (SF_{Mamp} and SF_{Namp}) for various aerosol loadings in the boundary layer with continental stratus and stratocumulus as the major cloud types. Hallberg et al. (1994) present lower SF_{Namp} (corresponding to intermediately and moderately polluted conditions) compared with the observations from Gillani et al. (1995, 1992) which may be explained by differing conditions at the sampling sites and/or underestimation due to the instrumentation used in the former case. The SF_{Mamp} and SF_{Namp} seen in Table 3 obviously decrease with the degree of pollution. Jensen and Charlson (1984) have also shown this feature in modelling studies for aerosol mass scavenging into convective clouds. It should be noted in Table 3 that the measured SF_{Namp} cover a wider range of values compared with SF_{Mamp}. Flossmann et al. (1985) predicted number scavenging efficiencies of between 48 to 94%, mainly confined to particles larger than 0.1 μm radius.

The measured scavenging fractions shown in Table 3 were mainly observed in stratiform clouds. Table 4 shows the scavenging fractions and uncertainties corresponding to the present classification. These values are estimated based on the relatively few observations presented in Table 3. The estimated SF_{Mamp} and uncertainty corresponding to clean conditions represent the mean and standard deviation (SD) obtained from calculations of the

Table 3. *Published data of observed SF_{Mamp} and SF_{Namp} for each classification*

Present classification	N_{amp} (cm^{-3})	SF_{Mamp} (%)	SF_{Namp} (%)	Cloud type	Reference
clean conditions	<500		84 ± 10	Cont. St, Sc	Gillani et al., 1995
			85 ± 11	Cont. St, Sc	Gillani et al., 1992
		87 ± 11	73 ± 7	Cont. St, Sc	Hallberg et al., 1994
		$90^{a} \pm 20$	60 ± 20	Cont. Sc, Co	Hegg and Hobbs, 1986[d]
		$\approx 96^{g}$		Marine St.	Frick and Hoppel, 1993
		95^{a}, 63^{b}, 97^{c}	77	Marine Sc	Noone et al., 2000
intermediately polluted conditions	500–1000		53 ± 28	Cont. St, Sc	Gillani et al., 1995
			70 ± 4	Cont. St, Sc	Gillani et al., 1992
		$64^{e} \pm 4$	$18^{e} \pm 2$	Cont. St, Sc	Hallberg et al., 1994
moderately polluted conditions	1000–3000		28 ± 5^{f}	Cont. St, Sc	Gillani et al., 1995
			52 ± 19	Cont. St, Sc	Gillani et al., 1992
		$42^{e} \pm 6$	$12^{e} \pm 2$	Cont. St, Sc	Hallberg et al., 1994
highly polluted conditions	>3000	≈ 20–30	≈ 1–10	Cont. Fog	Noone et al., 1992

[a] nss-$SO_4^=$ mass. [b] NO_3^- mass. [c] Classified based on below cloud mass concentrations of $SO_4^= = 0.5\ \mu g\ m^{-3}$ and $NO_3^- = 0.5\ \mu g\ m^{-3}$, instead of M_{amp} and N_{amp} are not observed. [e] These values are probably underestimated due to the instrumentation used. [f] The 25th and 75th percentiles. [g] This value might be overestimated.

Table 4. *Estimated SF_{amp} used in this study for the present classification*

Present classification	M_{amp} ($\mu g\ m^{-3}$)	N_{amp} (cm^{-3})	SF_{Mamp} (%)
clean conditions	0–2	<500	88 ± 12
intermediately polluted conditions	2–15	500–1000	76 ± 12
moderately polluted conditions	15–30	1000–3000	63 ± 23
highly polluted conditions	>50	>3000	30 ± 5

observed values of SF_{Mamp}, shown in Table 3. For the intermediately as moderately polluted conditions, in addition to the values of observed SF_{Mamp} obtained by Hallberg et al. (1994), the observed number scavenging fractions obtained by Gillani et al. (1995, 1992) have also been taken into consideration for these cases by assuming a conversion factor between SF_{Namp} and SF_{Mamp} for each classification. We expect that cloud type will be an important factor influencing scavenging efficiency. More convective clouds (Cu) are expected to have higher scavenging efficiencies than stratiform clouds under similar aerosol loadings. However, since nearly all the measurements in Table 3 are for stratiform clouds, the algorithm cannot yet explicitly account for cloud type.

4.3. Estimated mass to volume conversions

Table 5 shows estimated mean particle density and uncertainty for each classification based on measurements performed over the Northeast Atlantic, North Sea and in the Po Valley. Particle mass values shown in Table 5 have been converted from particle volume distributions which in turn were calculated from measured particle number distributions obtained using an optical particle counter. These results are compared with particle mass observations obtained from ion chromatography analysis of simultaneous filter samples.

For the clean case, Table 5 shows that nearly all of the total mass concentrations obtained using the PCASP consisted of ionic species. Therefore, for the first classification we have estimated the density of the accumulation-mode particles based only on possible combinations of the analysed nss-sulfate, ammonium and nitrate species. Ionic species contribute a large fraction of the mass concentrations in the intermediately polluted case as well. However, in this case we assume that also organic species have contributed with a fraction to the total mass concentrations which results in

Table 5. *Estimated mean particle density and uncertainty corresponding to each classification*

Present classification/ location	N_{amp} (cm^{-3})	Mass (OPC) ($\mu g\ m^{-3}$)		Mass (filter) ($\mu g\ m^{-3}$)					Estimated ρ_{amp} ($g\ cm^{-3}$)
		AMP	total	$nssSO_4^=$	NO_3^-	NH_4^+	CMP[e]	total	
clean conditions	<500								1.7 ± 0.1
NA[a] (26 June 1997)									
600 ft[f]	99 ± 8	0.6 ± 0.04	9 ± 1	0.7	0.8	0.06	6	8	
2600 feet	100 ± 12	0.6 ± 0.1	9 ± 3	0.8	0.8	0	6	9	
intermediately polluted conditions	500–1000								1.6 ± 0.2
NA (17 July 1997)	840 ± 226	10 ± 3	38 ± 8	11	2	3	12	29	
NA (17/18 July 1997)	608 ± 85	8 ± 1	25 ± 7	9	3	2	7	21	
moderately polluted conditions	1000–3000								1.6 ± 0.2
NS (9 March 1997)[b]	1189 ± 134	26 ± 2	54 ± 7	18	5	7	2	32	
NS (9 March 1997)[c]	1164 ± 56	25 ± 2	55 ± 5	17	3	6	2	28	
highly polluted conditions	>3000								1.4 ± 0.1
PV[d] (10 Nov. 1989)	≈ 5000			6				93	
PV (17 Nov. 1989)				13				179	

Particle mass values are converted from volume distributions which in turn are converted from particle number distributions measured below the clouds, obtained by the PCASP. Particle mass values are also obtained from ion chromatography analysis of simultaneous filters samples. For the highly polluted conditions, the total mass concentration are shown.

[a] NA = Northeast Atlantica. [b] North Sea (average over the time-period 12^{26}–13^{38}). [c] North Sea (average over the time-period 15^{12}–16^{17}). [d] Po Valley (Italy). [e] Coarse-mode particles. [f] Feet.

a lower value of the density than the previous case. For the moderately polluted case the ionic species were only slightly more than half of the total mass concentrations. Therefore, a significant fraction of organic species is assumed to have contributed to the mass in this case. From the highly polluted cases analysed filters were weighed before and after exposure and thus the total mass concentrations were obtained directly. Sulfate at this location accounted for less than 10% of the total mass. Therefore, a large fraction of organic species is assumed to have contributed to the aerosol mass for this case and thus a relatively low density of the aerosols is assumed for this classification.

Aerosol particles are in reality often externally mixed and represent a multi-component system where each chemical component has its own density. Typical densities of inorganic salts (sulfates, nitrates, chlorides, etc.) range from about 1.7 to 2.0 $g\ cm^{-3}$, while the densities of organic compounds range from slightly less than 1 to about 1.5 $g\ cm^{-3}$ (Hegg et al., 1995). The uncertainty induced by assuming a single value for the density of the accumulation-mode particles corresponding to each classification in the present approach is relatively small compared with the errors associated with other conversions in the algorithm (see Subsection 4.4).

4.4. Scavenged volume to droplet number

The last conversion, scavenged volume to droplet number, is the critical part in this approach. Fig. 2a shows examples of RSDs obtained by the CVI/PCASP in marine stratocumulus clouds. Fig. 2b shows the corresponding residual particle cumulative size distribution (CRSD) curves (dotted lines) and mean CRSD curve (solid line) converted from the individual RSDs and the mean RSD, respectively. The mean cumulative RSD for each classification is used in the present approach to find the Hatch–Choate parameters described below. By comparing Figs. 2a, b, one can see that

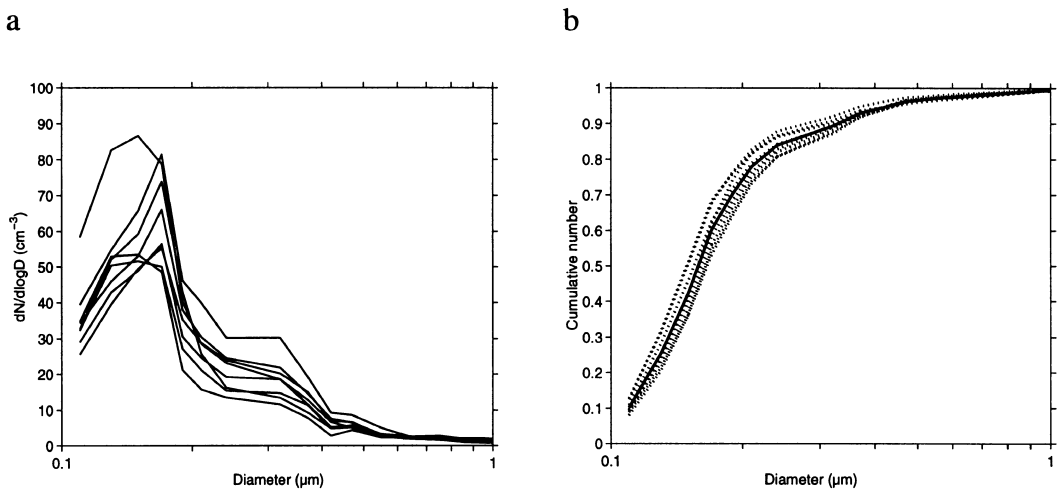

Fig. 2. Examples of residual particle size distributions obtained by the PCASP. The solid lines in Fig. 2a are examples of residual particle number size distribution (RSD) curves obtained by the PCASP. The dotted lines and solid line in Fig. 2b are residual particle cumulative size distribution (CRSD) curves and mean CRSD curve, respectively, converted from the individual RSDs shown in Fig. 2a and the corresponding mean RSD.

most of the variation in the residual size distributions is due to changes in total residual particle number, rather than changes in the shape of the residual particle distribution. The consistency in the shape of the residual distribution leads to relatively stable cumulative size distributions.

Fig. 3 shows cumulative residual size distributions which are subdivided according to our classification. The figure clearly shows that the median residual particle size increases with increasing aerosol loading in the clouds. As the level of pollution increases in the layer in which clouds form, larger particles become sufficiently abundant to account for the majority of the cloud droplets formed.

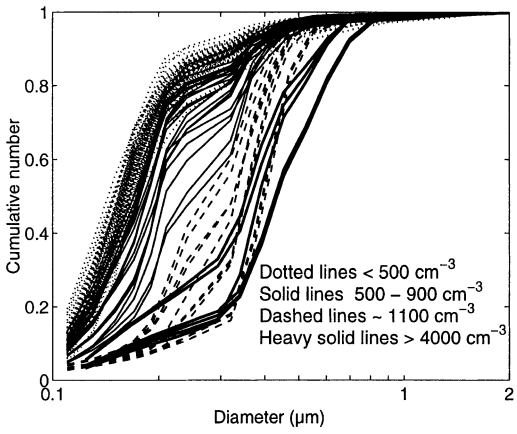

Fig. 3. The dotted, solid, dashed and heavy solid lines are cumulative residual size distributions curves, obtained by the PCASP, subdivided according the present classification.

Figs. 4a, b (the latter is an enlargement of Fig. 4a) illustrate how we obtain the parameters count median diameter (CMD) and geometric standard deviation (σ_g) from a mean cumulative RSD (heavy solid line). Count median diameter is defined as the diameter at which the cumulative distribution reaches 0.5 ($D_{50\%}$). We calculate σ_g as $D_{84\%}/D_{50\%}$. Figs. 4a, b also illustrate how we calculate deviations in $D_{50\%}$ and $D_{84\%}$ (dotted lines), converted from deviations of the mean cumulative RSD (dashed lines), and in σ_g. The dashed lines in Fig. 4 represent the standard deviations of the original residual number size distributions.

After finding the CMD and σ_g for each classification the next step in the present approach is to convert from the scavenged volume to residual particle number (thus cloud droplet number) using eq. (1), derived by Hatch and Choate. Deviations in the CMD and σ_g are propagated through the calculation and estimated deviations in the diameter of average volume are thus obtained.

$$\mathrm{DAV} = \mathrm{CMD}\, e^{1.5 \ln(\sigma_g)^2}. \quad (1)$$

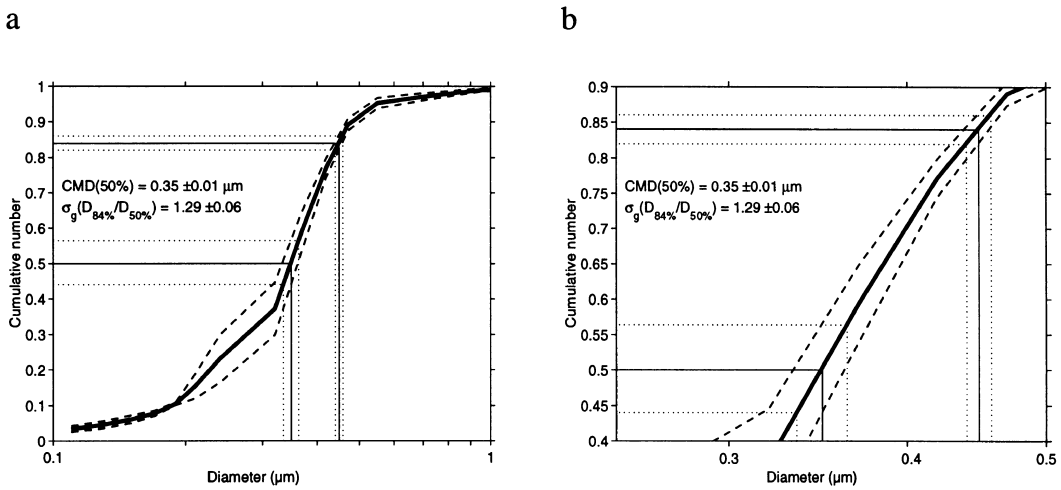

Fig. 4. Fig. 4b is an enlargement of Fig. 4a. The heavy solid line is a mean cumulative RSD curve. The dashed lines shown in Fig. 4 represent standard deviations of the original residual number size distributions. The figures illustrate how the present calculations of deviations in $D_{50\%}$ and $D_{84\%}$ (dotted lines), converted from deviations of the mean cumulative RSD (dashed lines), and in σ_g are performed.

To keep this conversion as simple as possible, we assume that the residual particle distributions can be adequately described using a unimodal lognormal distribution.

The cumulative RSDs shown in Fig. 3 are not perfectly lognormal size distributions. Uncertainties that are induced by using a single lognormal distribution rather than combining two (or more) lognormal distributions have not been formally estimated for all of the distributions. However, we can consider two cases to illustrate the kinds of uncertainty introduced by assuming a unimodal lognormal distribution.

Figs. 5a, b show RSDs observed in marine

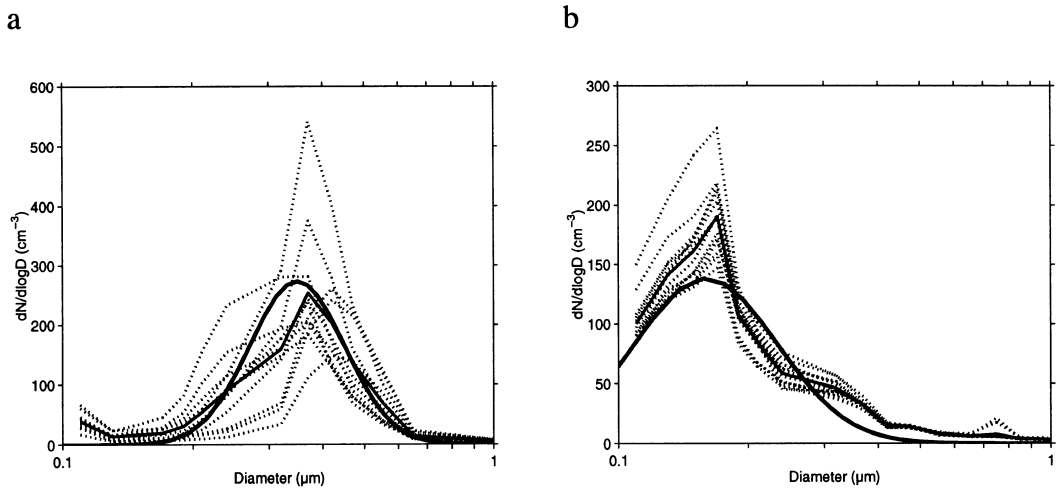

Fig. 5. The dotted lines in Fig. 5a, b are the RSD curves obtained by the PCASP from a moderately polluted day (North Sea, 9 March 1997) and a clean day (Northeast Pacific, 28 June 1994), respectively. The solid lines are the mean RSD curves. The heavy, solid lines are lognormal curves based on the Hatch–Choate parameters and the integrated number from each of the mean RSDs.

stratocumulus clouds during a moderately polluted day (North Sea, 9 March 1997) and a clean day (Northeast Pacific, 28 June 1994), respectively, compared with theoretical unimodal lognormal size distributions. The solid lines in the figures represent the mean measured RSD. The heavy solid line in each figure is a lognormal curve based on the Hatch–Choate parameters and the integrated number from each of the mean RSDs. Since the larger particles have the largest impact on the converted mass size distribution, we calculate σ_g as $D_{84\%}$ divided by $D_{50\%}$. For the North Sea case there is close correspondence between the mean measured RSD and the theoretical lognormal size distribution curve at the largest particle sizes. Thus, we expect the errors induced by assuming unimodal lognormal distribution for this case to be small. Considering the Northeast Pacific case shown in Fig. 5b, however, we see a larger difference between the mean measured RSD and the theoretical lognormal distribution. We will therefore induce a larger error in the conversion from scavenged aerosol volume to number for this cleaner case. Uncertainties also arise because the smaller part of the accumulation mode RSD in this case was not measured, an artifact that will affect the estimations of the CMD and σ_g, thus also the calculated diameter of average volume.

5. Results

5.1. Field and conversion summary

Table 6 shows a summary of the M_{amp} field and conversion values which are included in the present algorithm, subdivided based on our pollution level classification. The conversion algorithm for each pollution level class (i) can be expressed as:

$$N_{d,i} = \frac{M_{amp,i} SF_{amp,i}}{\rho_{amp,i} \frac{4}{3} \pi \left(\frac{DAV_i}{2} \right)^3}, \quad (2)$$

where $N_{d,i}$ is the cloud droplet number concentration, $M_{amp,i}$ is the accumulation-mode particle mass concentration, $SF_{amp,i}$ is the accumulation-mode particle mass scavenging fraction, $\rho_{amp,i}$ is the density of the accumulation-mode particles and DAV_i is the diameter of average volume for each classification.

The results in Table 6 together with eqs. (1) and (2) can be used to calculate the N_d field. Calculated N_d are based on the total volume scavenged into cloud droplets divided by the average volume of the scavenged aerosols (the right hand side of eq. (2)) and the assumption that each scavenged aerosol particle forms a single cloud droplet. Eq. (2) thus gives us the opportunity to estimate a relationship between accumulation-mode mass and cloud droplet number based on observable physical processes with the corresponding uncertainties involved.

5.2. Calculated cloud droplet concentrations compared with measured N_6

The present algorithm has been used for data from each of the 15 days that are included in this study to calculate N_d from M_{amp}. Table 7 shows a summary of the estimated M_{amp}, estimated conversion values and calculated N_d subdivided based on our pollution level classification. Estimated standard deviations in the N_d field are obtained by uncertainties propagated through the calculations. Table 7 also shows simultaneous independent measurements of N_d and corresponding SD for each case. Calculation of the SD for

Table 6. *Summary of the M_{amp} field, estimated conversion values which are included in the present algorithm, subdivided based on the present pollution level classification*

	M_{amp} ($\mu g\ m^{-3}$)	SF_{amp} (%)	±	ρ_{amp} ($g\ cm^{-3}$)	±	CMD (μm)	±	ρ_g	±
clean conditions	0–2	88	12	1.7	0.1	0.160	0.001	1.50	0.08
intermediately polluted conditions	2–15	76	12	1.6	0.2	0.190	0.001	1.82	0.03
moderately polluted conditions	15–50	63	23	1.6	0.2	0.35	0.01	1.29	0.06
highly polluted conditions	>50	30	5	1.4	0.3	0.42	0.07	1.4	0.3

Table 7. *Summary of the estimated M_{amp} estimated conversion values and calculated N_d for data from each of the 15 days that are included in this study, subdivided based on the present pollution level classification*

Present classification	Date	N_{amp} (cm^{-3})	M_{amp} ($\mu g\ m^{-3}$)	±	SF_{Mamp} (%)	±	ρ_{amp} ($g\ cm^{-3}$)	±	CMD (μm)	±	σ_g	±	N_d (cm^{-3})	±	${}_{obs}N_d$ (cm^{-3})	±
clean conditions	8 June 1994	59	0.76	0.22	88	12	1.7	0.1	0.164	0.005	1.9	0.2	28	23	58	25
	11 June 1994	246	2.0	0.3	88	12	1.7	0.1	0.165	0.001	1.42	0.003	260	56	238	43
	12 June 1994	32	0.55	0.18	88	12	1.7	0.1	0.165	0.001	1.5	0.1	55	24	28	9
	27 June 1994	133	1.1	0.2	88	12	1.7	0.1	0.156	0.001	1.51	0.01	140	31	166	29
	28 June 1994	125	1.2	0.2	88	12	1.7	0.1	0.16	0.001	1.46	0.01	160	34	201	28
	29 June 1994	31	0.33	0.05	88	12	1.7	0.1	0.159	0.001	1.53	0.06	37	10	57	15
	30 June 1994	93	1.1	0.1	88	12	1.7	0.1	0.159	0.007	1.8	0.2	51	35	174	33
	22 June 1997	198	1.8	0.7	88	12	1.7	0.1	0.17	0.002	1.55	0.08	150	73	193	64
	26 June 1997	100	0.60	0.09	88	12	1.7	0.1	0.147	0.001	1.42	0.01	110	23	66	13
intermediately polluted conditions	17 July 1997	840	10	3	76	12	1.6	0.2	0.195	0.001	1.8	0.1	250	120	229	52
	17/18 July 1997[a]	608	7.6	1.3	76	12	1.6	0.2	0.181	0.001	1.8	0.2	250	100	280	57
	18 July 1997	577	7.0	0.4	76	12	1.6	0.2	0.179	0.002	1.9	0.1	150	80	229	81
moderately polluted conditions	9 March 1997	1178	26	2	63	23	1.6	0.2	0.35	0.01	1.29	0.06	340	150	389	63
highly polluted conditions	10 Nov. 1989	~5000	93	10	30	5	1.4	0.3	0.372	0.003	1.44	0.01	400	100	274	125
	17 Nov. 1989		179	18	25	5	1.4	0.3	0.4327	0.0005	1.448	0.003	400	120	557	125

Estimated standard deviations in the N_d field are obtained by deviations propagated through the calculations. Observed N_d for each days were obtained independently by FSSP instruments.

[a] Night flight.

each case is based on 1 Hz data. For the clean to moderately polluted conditions, N_d measurements were performed with FSSP instruments mounted on the British Meteorological Research Flight (MRF) C-130 and University of Washington (UW) C-131 research aircraft, on which CVIs were also deployed. For the two most polluted cases (the highly polluted conditions) fog droplets larger than 1 μm in diameter were measured with a land-based FSSP (Noone et al., 1992). About 98% of the liquid water content were found in droplets larger than 3 μm in diameter. Therefore, the results shown in Table 7 include fog droplets larger than this size.

Fig. 6 shows the calculated N_d as a function of the M_{amp} (stars) based on data from Table 7. Fig. 6 also shows a least-squares fit (solid line) for the calculated N_d values having a correlation coefficient (r^2) of 0.85. Simultaneous independent measurements of N_d (circles) performed with the FSSP instruments are also shown for each case. The agreement between calculated and observed N_d values is, with one exception (the result of N_d based on data from 30 June 1994, and marked with an arrow in Fig. 6), within a factor of 2 and for many of these cases also much better than a factor of 2. The corresponding calculated and observed values of SD are for both cases relatively large.

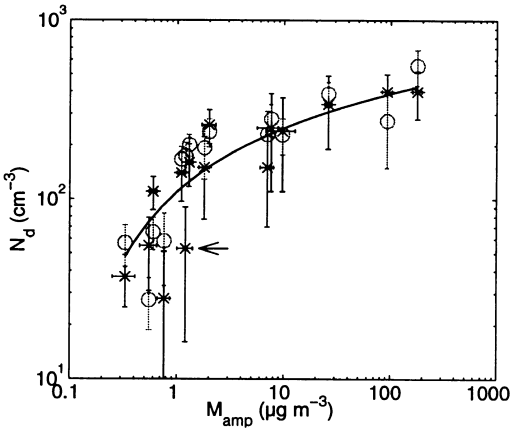

Fig. 6. The calculated N_d marked with stars (based on data from Table 7) are obtained by the method presented in this study. Estimated standard deviations in the N_d field are obtained by uncertainties propagated through the calculations. The solid line is a least-squares fit for the calculated N_d values having a correlation coefficient (r^2) of 0.85. The measured N_d marked with circles and the corresponding SD, based on 1 Hz data, were obtained by FSSP instruments. The star marked with an arrow is discussed in the text.

5.3. *Calculated N_d compared with earlier empirical studies*

We can compare results using the present algorithm with previous studies relating sulfate mass and cloud drop number. Fig. 7 shows the calculated N_d (stars) and the least-squares fit (solid line) for the data (the same as in Fig. 6) compared with empirical estimations of N_d from studies by Jones and Slingo (large circles), Hegg (small circles), and Boucher and Lohmann (plus-symbols), respectively. The three latter relationships are used to calculate N_d from measured or derived $SO_4^=$ mass. All four methods produce similar results for aerosol masses above roughly 1 μg m^{-3}. The present algorithm produces N_d values that are consistently lower than the three previous studies at aerosol mass values below 1 μg m^{-3}. We see that the

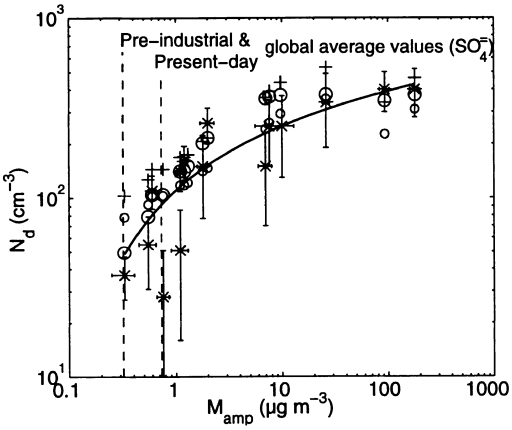

Fig. 7. The calculated N_d marked with stars (based on data from Table 7) are obtained by the method presented in this study. Estimated standard deviations in the N_d field are obtained by uncertainties propagated through the calculations. The solid line is a least-squares fit for the calculated N_d values having a correlation coefficient (r^2) of 0.85. The estimated N_d marked with large circles, small circles and plus-symbols are obtained by Jones and Slingo (1996), Hegg (1994), and Boucher and Lohmann (1995), respectively. The vertical dashed lines denote the pre-industrial and present day global average sulfate mass values from model calculations (Jones and Slingo, 1996).

relationship from this study is in best agreement with the results by Jones and Slingo.

The vertical dashed lines in Fig. 7 denote the pre-industrial and present day global average sulfate mass values from model calculations (Jones and Slingo, 1996). Due to the inherent nonlinearity in the relationship between N_d and M_{amp}, cloud droplet number will be most sensitive to changes in aerosol mass loading at the lowest mass concentrations. Since the slope of the relationship is largest between these mass values for our algorithm and the Jones–Slingo method, we expect that these two will result in a larger indirect forcing estimates compared with the studies by Hegg (1994) and Boucher and Lohmann (1995). By comparing average values of estimated effective radius for the present-day conditions the present calculations of N_d shown in Fig. 7 indicate that our algorithm produces results in closest agreement with results by Hegg (1994) and Jones and Slingo (1996). A comparison of predicted mean effective radius, from the Jones and Slingo (1996), Hegg (1994), and Boucher and Lohmann (1995) studies for present-day conditions shows that the parameterisations of Jones et al. (1994) and Hegg (1994) are quite similar to each other and are in general closer to satellite retrievals (a single data source from Han et al. (1994)) than the simulation using the parameterisation by Boucher and Lohmann (1995).

5.4. *Uncertainty ranking*

The relatively sparse data set with which we have developed the present algorithm only allows us to classify the aerosol mass field into 4 categories. The coarseness of this classification results in uncertainties that need to be recognized when using the algorithm in model calculations. A major difficulty with the present classification scheme is that the droplet number calculated for mass values in different categories is not unique. Fig. 8 shows the droplet number concentrations calculated for a range of aerosol mass values within each category. As an extreme example, one would obtain an N_d value of 188 cm^{-3} for an aerosol mass concentration of 1.9 $\mu g\, m^{-3}$ (close to the maximum value in the "clean" category) and a value of 45 cm^{-3} for a mass value of 2.1 $\mu g\, m^{-3}$. While the results shown in Figs. 6, 7 clearly show that the algorithm produces reasonable results, care must be taken in applying the algorithm, especially when aerosol mass values are near the borders of the classification categories.

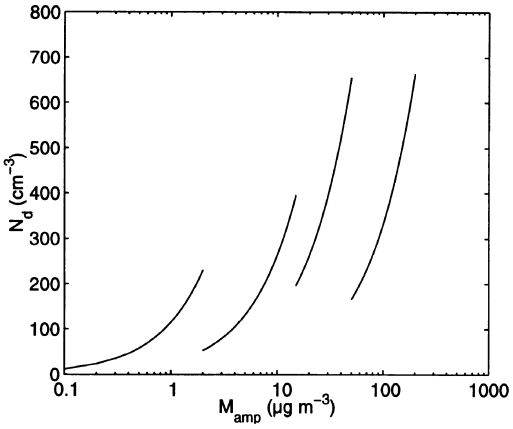

Fig. 8. N_d are calculated based on the results shown in Table 6 and for a range of aerosol mass values within each category.

There are 2 ways of circumventing this difficulty. The first is to simply use the least-squares fit to the data to calculate N_d (cm^{-3}) from M_{amp} ($\mu g\, m^{-3}$): $N_d = 87 \log_{10}(1 + (M_{amp}/0.32)^2)$. A disadvantage with using the least-squares fit is that the direct link to the physical process inherent in the algorithm is lost. While this least-squares approach may be useful in the short-term, it is not acceptable as a long-term solution since the major point with developing this algorithm is so that all of the conversions can be based on observable physical processes.

The longer-term solution is to obtain more data for scavenging fractions, particle chemical composition and density, and residual particle size distributions as a function of aerosol mass loading and cloud type. More data of this kind will allow a finer classification scheme to be developed, and allow the algorithm to retain its direct link to real physical processes.

The scatter occurring in the calculated N_d shown in Fig. 6 is probably largely due to the sensitivity in the conversion from scavenged volume to cloud droplet number. The calculated DAV, based on observed CMD and σ_g, is raised to a power of 3 in equation (2). An examination of the two case studies in Subsection 4.5.3 suggests that data from days classified as clean seems to be more sensitive

in the present approach than the more anthropogenically influenced days. Dynamical processes (e.g., cloud type) not accounted for in the algorithm may also induce some of the scatter shown in Figs. 6, 7 for the aerosol mass/droplet number relationship, especially for the clean conditions.

Furthermore, uncertainties are induced in the estimations of the present M_{amp} field and data from the days classified as clean seem to be more sensitive than the more anthropogenically influenced cases. For data corresponding to a higher aerosol loading, the volume spectra obtained by the CVI/PCASP is described by a bimodal distribution with nearly complete separation of the accumulation- and course-mode particles. However, for clean cases the volume spectra is described by a nearly unimodal course-mode distribution where the accumulation-mode particles exhibit a tail at the smallest sizes. So, for the latter case it is more difficult to separate the accumulation mode from the course mode compared with a higher aerosol loading. Here the errors induced by estimating M_{amp} could be significant.

6. Summary and conclusions

In this study, we present droplet number fields calculated from accumulation-mode aerosol mass fields using a conversion algorithm in which each step in the conversion scheme is based on real physical processes that occur in the atmosphere and can be observed or modeled. The present algorithm is developed based on a relatively sparse data set and our classification therefore induce uncertainties that need to be recognized when using the algorithm in model calculations. The quantities σ_g and CMD are probably responsible for much of the inconsistent results of N_d that occur near the boundaries of the four classification categories. To improve the algorithm in the longer-term requires more data of scavenging fractions, particle chemical composition and density, and residual particle size distributions as a function of aerosol mass loading and cloud type.

The algorithm has been used on data from 15 days and the agreement between calculated and observed N_d values is, with one exception, within a factor of 2 and for many of these cases also much better than a factor of 2. Based on the study by Slingo (1990), the fact that the algorithm can predict N_d values that are usually within a factor of 2 of observations shows that it can be applied in climate models. However, in the Slingo (1990) study, a doubling of cloud droplet number could offset the entire 2.5 W m^{-2} forcing due to anthropogenic greenhouse gases. To be more useful in climate model estimations, further work on the algorithm must be done to improve both its accuracy and precision. In addition to the results of the algorithm itself, we also present a least-squares fit to the predicted N_d values. While this approach has the advantage of producing a unique N_d for all values of M_{amp}, it has the major disadvantage of losing the direct relationship to physical processes inherent in the algorithm itself. In the short-term this approach may, however, be useful.

The largest errors induced seem to occur for the days classified as clean mainly due to uncertainties induced in the conversion between scavenged volume and droplet number. Dynamical processes not accounted for in the algorithm may, especially for clean conditions, also induce some of the scatter seen in the results.

The present result seems to be in closest agreement with the estimation by Jones and Slingo (1996), compared with the studies by Hegg (1994) and Boucher and Lohmann (1995), to predict the indirect forcing. The calculated N_d based on M_{amp} presented in this study seem to result in estimated average value of effective radius for the present-day condition close to the results by Hegg (1994) and Jones and Slingo (1996).

Finally, this study suggests that other species other than sulfate are important for the formation of cloud droplets.

7. Acknowledgments

We would like to thank the pilots, captains and crews of the UW C-131 and MRF C-130 for their excellent work during the field campaigns. We would also like to thank the MRF scientists for their collaboration during the ACE-2 campaign and for patiently working up data used in this study. Finally, thanks to Klaus Wyser for useful discussions. The work has been financed through research grants from European Commission (ENV4-CT95-0032) and from the office of Naval Research (grant # 2503–1993).

REFERENCES

Albrecht, B. A. 1989. Aerosols, cloud microphysics, and fractional cloudiness. *Science* **245**, 1227–1230.

Boucher, O. and Lohmann U. 1995. The sulfate–CNN–cloud albedo effect. *Tellus* **47B**, 281–300.

Flossmann, A. I., Hall, W. D. and Pruppacher, H. R. 1985. A theoretical study of the wet removal of atmospheric pollutants. Part 1: The redistribution of aerosol particles captured nucleation and impaction scavenging by growing cloud drops. *J. Atmos. Sci.* **42**, 583–606.

Frick, G. M. and Hoppel, W. A. 1993. Airship measurements of aerosol size distributions, cloud droplet spectra, and trace gas concentrations in the marine boundary layer. *Bull. Amer. Meteor. Soc.* **70**, 354–365.

Gillani, N. V., Daum, P. H., Schwartz, S. E., Leaitch, W. R., Strapp, J. W. and Isaac, G. A. 1992. Fractional activation of accumulation-mode particles in warm continental stratiform clouds. In: *Precipitation scavenging and atmospheric-surface exchange processes*, vol. 1, edited by Schwartz, S. E. and Slinn, W. G. N., pp. 345–358, Hemisphere Bristol, Pa.

Gillani, N. V. and Schwartz, S. E. 1995. Field observations in continental stratiform clouds: Partitioning of cloud particles between droplets and unactivated interstitial aerosols. *J. Geophys. Res.* **100**, **D9**, 18,687–18,706.

Hallberg, A., Ogren, J. A., Noone, K. J., Heintzenberg, J., Berner, A., Solly, I., Kruisz, C., Reischl, G., Fuzzi, S., Facchini, M. C., Hansson, H.-C., Wiedensohler, A. and Svenningsson, I. B. 1992. Phase partitioning for different aerosol species in fog. *Tellus* **44B**, 545–555.

Hallberg, A., Noone, K. J., Ogren, J. A., Svenningsson, I. B., Flossmann, A. I., Wiedensohler, A., Hansson, H.-C., Heintzenberg, J., Anderson, T. L., Arends, B. G. and Maser, R. 1994. Phase partitioning of aerosol particles in clouds at Kleiner Feldberg. *J. Atmos. Chem.* **19**, 107–127.

Han, Q., Rossow, W. B. and Lacis, A. A. 1994. Near-global survey of effective droplet radii in liquid water clouds using ISCCP data. *J. Climate* **7**, 475–497.

Hatch, T. and Choate, S. P. 1929. Statistical description of the size properties of non-uniform particulate substances. *J. Franklin Inst.* **207**, 369.

Hegg, D. A. 1994. Cloud condensation nucleus–sulfate mass relationship and cloud albedo. *J. Geophys. Res.* **99**, **D12**, 25,903–25,907.

Hegg, D. A. and Hobbs, P. V. 1986. Sulfate and nitrate chemistry in cumuliform clouds. *Atmos. Environ.* **20**, 901–909.

Hegg, D. A., Ronald, F. J. and Hobbs, P. V. 1993. Light scattering and cloud condensation nucleus activity of sulfate aerosol measured over the Northeast Atlantic Ocean. *J. Geophys. Res.* **98**, **D8**, 14,887–14,894.

Hegg, D. A., Hobbs, P. V., Ronald, F. J. and Waggoner, A. P. 1995. Measurements of some aerosol properties relevant to radiative forcing on the east coast of the United States. *J. Applied Meteorology* **34**, 2306–2315.

IPCC. 1995. *Climate change 1995: the science of climate change*. J. T. Houghton, L. G. Meria Filho, B. A. Callander, N. Harris, A. Kattenberg and K. Maskell (eds.). Cambridge University Press, Cambridge, UK.

Jensen, J. B. and Charlson R. J. 1984. On the efficiency of nucleation scavenging. *Tellus* **36B**, 367–375

Jones, A., Roberts, D. L. and Slingo, A. 1994. A climate model study of indirect radiative forcing by anthropogenic sulphate aerosols. *Nature* **370**, 450–453.

Jones, A. and Slingo, A. 1996. Predicting cloud-droplet effective radius and indirect sulphate aerosol forcing using a general circulation model. *Q. J. R. Meteorol. Soc.* **122**, 1573–1595.

Martin, G. M., Johnson, D. W. and Spice, A. 1994. The measurement and parametrisation of effective radius of droplets in warm stratocumulus clouds. *J. Atmos. Sci.* **51**, 1823–1842.

Noone, K. J., Ogren, J. A., Heintzenberg, J., Charlson, R. J. and Covert, D. S. 1988. Design and calibration of a counterflow virtual impactor for sampling of atmospheric fog and cloud droplets. *Aerosol Sci. Tech.* **8**, 235–244.

Noone, K. J., Ogren, J. A., Hallberg, A., Heintzenberg, J., Ström, J., Hansson, H.-C., Svenningsson, B., Wiedensohler, A., Fuzzi, S., Facchini, M. C., Arends, B. G. and Berner, A. 1992. Change in aerosol size- and phase distributions due to physical and chemical processes in fog. *Tellus* **44B**, 489–504.

Noone, K. J., Öström, E., Ferek, R. J., Garrett, T., Hobbs, P. V., Johnson, D. W., Taylor, J. P., Russell, L. M., Flagan, R. C., Seinfeld, J. H., O'Dowd, C. D., Smith, M. H., Durkee, P. A., Nielson, K., Hudson, J. G., Pockanly, R. A., DeBock, L., Van Grieken, R., Gasparovic, R. F. and Brooks, I. 2000. A case study of ships forming and not forming tracks in moderately polluted clouds. *J. Atmos. Sci.* **57**, 2729–2747.

Novakov, T. and Penner, J. E. 1993. Large contribution of organic aerosols to cloud-condensation-nuclei concentrations. *Nature* **385**, 823–826.

O'Dowd, C. D. and Smith, M. H. 1993. Physiochemical properties of aerosols over the Northeast Atlantic. Evidence for wind-speed-related submicron sea-salt aerosol production. *J. Geophys. Res.* **98**, 1137–1149.

Ogren, J. A., Heintzenberg, J. and Charlson, R. J. 1985. In-situ sampling of clouds with a droplet to aerosol converter. *Geophys. Res. Lett.* **12**, 121–124.

Pueschel, R. F. and Van Valin, C. C. 1986. Aerosol in polluted versus nonpolluted air masses: long-range transport and effects on clouds. *J. Climat. Appl. Meteor.* **25**, 1908–1917.

Quinn, P. K., Marshall, T. S., Covert, D. S. and Kapustin, V. N. 1995. Comparison of measured and calculated aerosol properties relevant to the direct radiative for-

cing of tropospheric sulfate aerosol on climate. *J. Geophys. Res.* **100**, **D5**, 8977–8991.

Rivera-Carpio, C. A., Corrigan, C. E. and Novakov, T. 1996. Derivation of contributions of sulfate and carbonaceous aerosols to cloud condensation nuclei from mass size distributions. *J. Geophys. Res.* **101**, **D14**, 19,483–19,493.

Russell, L. M., Noone, K. J., Ferek, R. J., Pockalny, R. A., Flagan, R. C. and Seinfeld, J. H. 2000. Combustion organic aerosol as cloud condensation nuclei in ship tracks. *J. Atmos. Sci*., in press.

Seinfeld, J. H. and Pandis, S. N. *Atmospheric chemistry and physics: from air pollution to climate change*, 1326 pp. John Wiley & Sons Inc., New York, 1998.

Slingo, A. 1990. Sensitivity of the Earth's radiation budget to changes in low clouds. *Nature* **343** (6253), 49–51.

Twomey, S. A. 1977. *Atmospheric aerosols*. Elsevier Scientific Publishing Co., Amsterdam, 302 pp.

Twomey, S. A., Piepgrass, M. and Wolfe, T. L. 1984. An assesment of the impact of pollution on global cloud albedo. *Tellus* **36B**, 356–366.